Chapter 11
Metrology Based on Chaotic Semiconductor Lasers

On the way to chaotic evolution, periodicity, bistability, and multistability are observed, such as in the outputs of semiconductor lasers with optical feedback. The system of optical feedback in a semiconductor laser is sometimes called self-mixing semiconductor laser. In a periodic state, the laser output shows not simply periodic oscillation but also hysteresis. Novel applications have been proposed based on these phenomena, for example, a displacement measurement is performed by counting the fringes obtained from bistable self-mixing interference between the internal field and the optical feedback light in the laser cavity. The direction of the displacement is simultaneously determined from asymmetric waveforms showing hysteresis. Also correlation of signals between scattering and reference chaotic lights can be applied for remote sensing from distant reflecting targets. We discuss various methods for optical metrology based on self-mixing interference effects and correlation techniques in semiconductor lasers. This chapter does not deal with the detailed descriptions of the methods and their accuracies but with the introduction of the principles of the methods.

11.1 Optical Feedback Interferometers

11.1.1 Bistability and Multistability in Feedback Interferometers

Laser interferometry is a well-established technique for the measurement of vibrations and displacement of objects. In the interferometry, for example, the displacement of the order of optical wavelength is measured from the fringe analysis of sinusoidal variations of signals from the interferometer output. We have investigated the self-mixing effects in semiconductor lasers with optical feedback in Chap. 4. We have also shown that the laser output exhibited periodic undulations with half of the optical wavelength for the change of the external cavity length under an appropriate condition of the external reflectivity. In self-mixing semiconductor lasers, the returned light from an external reflector interferes with the internal laser oscillation

J. Ohtsubo, *Semiconductor Lasers*, Springer Series in Optical Sciences 111,
DOI: 10.1007/978-3-642-30147-6_11, © Springer-Verlag Berlin Heidelberg 2013

and the original field in the laser cavity plays a role for the reference wave. Therefore, we can conduct interferometic measurements using semiconductor lasers with optical feedback based on the same principle as the ordinary laser interferometers and we can obtain the absolute position, displacement, and vibration of the external reflector.

In this interferometric measurement, we use periodic oscillations, especially period-1 states, prior to chaotic oscillations on the way to period doubling bifurcations. Since self-mixing in semiconductor lasers is a nonlinear effect, not only the absolute value of the displacement but also the additional information of the direction of motion (whether the object is approaching or is going away from the laser) can be easily determined from the analysis for the fringe pattern. A semiconductor laser itself plays a role not only as a light source but also as a self-mixing detector in the measurement. In commercially available semiconductor lasers, a photo-diode is usually installed within the laser package as a monitor of the laser output power and we can use it as a detector for the fringe analysis. Therefore, we can construct a very compact sensor for the interferometic measurements. Also, we do not require complex processing for the post-detection signal. However, it is noted that the technique is limited to a certain range of the reflectivity of the external reflector. For large reflectivity of the external reflector, the detected signal may not be a periodic oscillation but a chaotic irregular oscillation. We cannot apply the method for such a case of a large reflectivity of the external reflector.

In the following, we investigate the interferometric measurements using bistable states (period-1 states) of light outputs in self-mixing semiconductor lasers discussed in Chap. 4. The optical configuration is the same as that in Fig. 4.1 and the rate equations of the model are given by (4.5)–(4.7). In the presence of optical feedback in a semiconductor laser, the oscillation angular frequency changes from ω_0 (the solitary oscillation) to ω_s. The relation between the two angular frequencies is given by

$$\omega_0 \tau = \omega_s \tau + C \sin(\omega_s \tau + \tan^{-1} \alpha) \tag{11.1}$$

where $C = \kappa \tau \sqrt{1+\alpha^2}/\tau_{\text{in}}$. The dynamics in semiconductor lasers subjected to optical feedback strongly depend on the C parameter. We are interested in the parameter region of $C \sim 1$ in this chapter, where the laser shows periodic states prior to the onset of chaotic oscillations. Using (4.9)–(4.11), the steady-state value of the laser output is given by

$$S_s = A_s^2 = \frac{\frac{\tau_s J}{ed} - n_s + \frac{2\kappa}{G_n \tau_{\text{in}}} \cos \omega_s \tau}{1 - \frac{2\kappa \tau_{\text{ph}}}{\tau_{\text{in}}} \cos \omega_s \tau} \frac{\tau_{\text{ph}}}{\tau_s} \tag{11.2}$$

Since we are considering a rather small coefficient κ of optical feedback, the difference between the laser output powers with and without optical feedback is small. Then, the difference can be approximated as follows:

$$\Delta S = S_s - S_s|_{\kappa=0} \approx \Delta S_0 \cos \omega_s \tau \tag{11.3}$$

where $\Delta S_0 = 2\kappa\tau_{ph}^2(J/ed - n_s/\tau_s)/\tau_{in}$. In actual fact, ΔS is a time dependent function because the carrier density also varies with time by the optical feedback. We introduce a normalized function $F(t)$ as $F(t) = \Delta S(t)/\Delta S_0$. Substituting (11.3) into (11.1) and using the relation $\omega_0\tau = 2kL$, the external cavity length as a function of time t is given by

$$
\begin{aligned}
&L(t) = \frac{1}{2k}\left[\cos^{-1} F(t) + \frac{C}{\sqrt{1+\alpha^2}}\left\{\alpha F(t) + \sqrt{1-F^2(t)}\right\} + 2m\pi\right] \\
&\frac{\mathrm{d}F}{\mathrm{d}t}\cdot\frac{\mathrm{d}L}{\mathrm{d}t} < 0 \\
&L(t) = \frac{1}{2k}\left[-\cos^{-1} F(t) + \frac{C}{\sqrt{1+\alpha^2}}\left\{\alpha F(t) - \sqrt{1-F^2(t)}\right\} + 2(m+1)\pi\right] \\
&\frac{\mathrm{d}F}{\mathrm{d}t}\cdot\frac{\mathrm{d}L}{\mathrm{d}t} > 0
\end{aligned}
\tag{11.4}
$$

where m is a non-negative integer number ($m = 0, 1, 2, \ldots$). The laser output varies for the change of the external cavity length, but the waveform has asymmetric features depending whether the external reflector moves toward or away from the laser. Then, we can determine the displacement of the external reflector and also the direction of movement in accordance with the relation in (11.4).

Next, we investigate the effect of optical feedback at bistable states of the laser output power. For a small optical feedback of $C = 0.6$, for example, the laser output power is a periodic oscillation as shown in Fig. 11.1a and the period is just half of the optical wavelength (Donati et al. 1995). The variation of the waveform is smooth, but it is not a symmetrical shape as expected from the above discussion. In this numerical simulation, it is assumed that the external mirror is moving away from the laser, i.e., the phase $\omega_0\tau$ is increasing. If the phase $\omega_0\tau$ is decreasing, the laser output shows the reversed waveform to Fig. 11.1a. Therefore, we can determine the direction of the movement from the shape of the waveform. For a large value of a C parameter of $C = 3$, the laser output power still varies with the period of $\lambda/2$, but shows hysteresis as shown in Fig. 11.1b. At this parameter value, the laser output power takes bistable states for a certain range of the phase. Therefore, we can expect a significant difference between the shapes of the waveforms for the increase or decrease of the external mirror position. With further increase of the C parameter value, skew of the waveform is enhanced and the laser output takes multi-stable states. These multi-stable states are rarely observed in actual situations and the laser behaves as the chaotic oscillations under these conditions, since multi-stable states are usually "unstable" in real systems.

Figure 11.2 presents the experimental results of self-mixing signals for different optical feedback strengths (Giuliani et al. 2001). The external reflector is put on a loudspeaker and the loudspeaker is driven by a sinusoidal signal in Fig. 11.2a. When the feedback is small in Fig. 11.2b (the feedback strength in intensity is roughly estimated as 10^{-7}), the laser output power shows a periodic undulation whose period is equal to half of the optical wavelength. In Fig. 11.2c (the feedback strength of 10^{-5}),

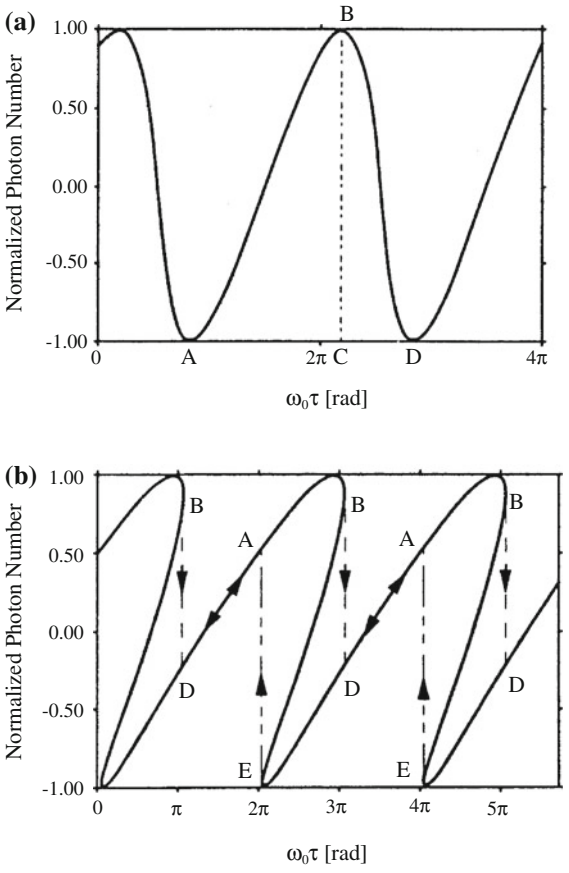

Fig. 11.1 Numerical calculation of laser output power ΔS for phase $\omega_0\tau$. **a** $C = 0.6$ and **b** $C = 3$ with hysteresis. The linewidth enhancement factor is chosen as $\alpha = 6$ [after Donati et al. (1995); © 1995 IEEE]

the laser output power is quite different from the periodic state in Fig. 11.2b. The waveform is still periodic, but the waveform for the increase of the phase is completely different from that for the decrease. Then, the absolute value of the displacement of the external reflector is obtained by counting the peaks of the undulations in the waveform and the direction of the movement is clearly discriminated by examining the waveform. The feedback intensity of 10^{-5} corresponds to the periodic state just before the onset of chaotic evolution in a semiconductor laser with optical feedback. For the large feedback strength of 10^{-4} in Fig. 11.2d (corresponding to a moderate to strong feedback in regime IV), the coherence of the laser is completely destroyed and periodicity is not visible in the waveform. As a result, the laser output power exhibits a similar waveform to the driving signal. However, the signal is broadened due to the modulation of fast chaotic oscillations. It is also noted that the offset phase of the signal is generally not always equal to that of the driving signal.

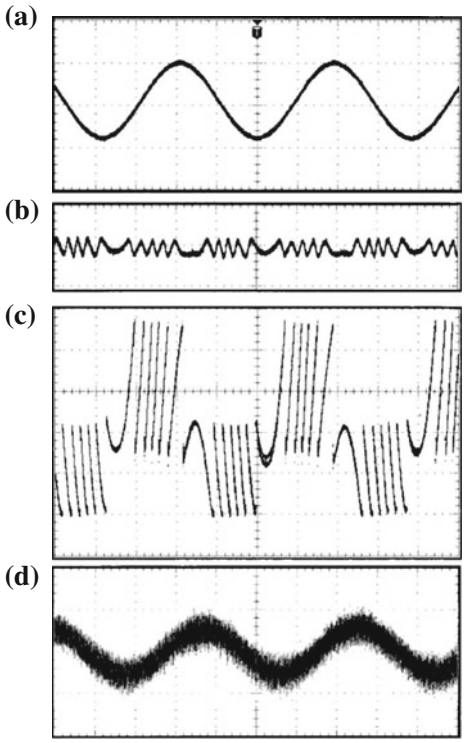

Fig. 11.2 Experimentally observed self-mixing signals for a change of external reflector. **a** Driving sinusoidal signal of external reflector. Laser output signals for external reflectivities of **b** 10^{-7} with periodic state, **c** 10^{-5} with hysteresis, **d** 10^{-4} with coherence collapse state. The driving signal corresponds to the change of the external reflector for 1.3 μm/div. The oscillation wavelength of the laser used is 800 nm. The time scale is 1 ms/div [after Giuliani et al. (2001); © 2001 SPIE]

11.1.2 Interferometric Measurement in Self-Mixing Semiconductor Lasers

We can measure the change of the external cavity length on the order of half of the optical wavelength by using the self-mixing effect in semiconductor lasers and also determine the direction of the change. Based on these principles, we here discuss the concrete methods for the measurement of displacement, vibration, and absolute position of the external reflector. Each measurement includes a particular processing algorithm for the detected signals, however, the fundamental methods of signal processing for those measurements still contain the common technique (Donati et al. 1995). Before discussing each technique, we take the measurement for the displacement of an external reflector as an example and show the detection and analysis for periodic signals in the self-mixing laser output. Figure 11.3 is an example of the signal processing systems. The light reflected from a target mirror is mixed with the original laser field in the laser cavity and the mixed signal is detected by a photodiode installed in the laser package. The detected signal passes through an amplifier and a high-pass filter. Then, the up- and down-edges of the periodic signal for every $\lambda/2$ period are counted by a counter. As a result, the displacement

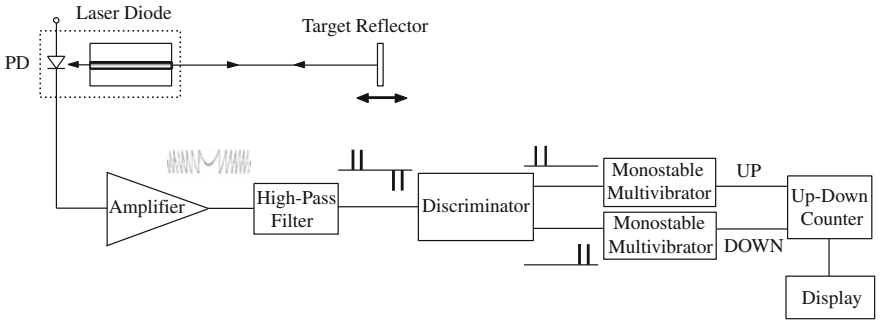

Fig. 11.3 Basic circuits of signal processing for interferometric measurements in self-mixing semiconductor lasers

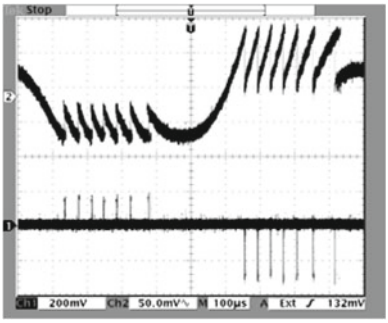

Fig. 11.4 *Upper trace*: experimental self-mixing signal obtained for a sinusoidal target displacement of 3.3 µm peak-to-peak amplitude and 1 kHz frequency, *lower trace*: analogue derivative of self-mixing signal, showing up/down-pulses. The timescale is 100 µs per division [after Giuliani et al. (2002); © 2002 IOP]

of the target reflector including the direction of the movement during the counting is calculated. The basic resolution of the measurement is $\lambda/2$ in this technique. It is noted that the SNR of the self-mixing interferometer using semiconductor lasers is limited by the efficiency of the coupling photodiode, and it is about 20 dB poorer than of conventional interferometry with the 50/50 half mirror (Giuliani et al. 2002). However, we can construct a very simple measurement system with high flexibility by the self-mixing interferometer using semiconductor lasers. In the following discussions, we assume that the laser output due to the mixing is a periodic signal with period $\lambda/2$ without notice.

In the following, we show typical signals observed in the self-mixing semiconductor lasers. We take an example of the displacement measurement of an external target under an appropriate condition of the external optical feedback for bistability operation of $C > 1$. Figure 11.4 is an experimental self-mixing signal for a sinusoidal displacement of the object. In the figure, the upper trace is the experimental self-mixing signal for a sinusoidal target displacement of 3.3 µm peak-to-peak amplitude and 1 kHz frequency. The lower trace is an analogue derivative of a self-mixing signal, showing up- and down-pulses, where the states of up- and down-pulses correspond whether the target is coming toward or going away from the laser. By

this approach, displacement of retro-reflective target has been successfully measured over 1 m distance with an allowed maximum speed of 0.4 m/s, solely limited by electronic bandwidth. The maximum target distance is limited by the coherence length of semiconductor lasers, being usually several meters to 10 meters. For an appropriate target reflectivity satisfying the condition $C > 1$, the self-mixing signal becomes a sawtooth-like waveform and, then, an accuracy better than $\lambda/2$ can be achieved by linearization of the interferometric fringe, i.e., the function defined in (11.4) is approximated by ideal sawtooth. A resolution of 65 nm has been achieved using a semiconductor laser with a wavelength of 780 nm, in which the resolution is improved by a factor of 6 with respect to conventional fringe counting technique (Servagent et al. 1998). Residual inaccuracy is caused by the nonlinearity of the actual self-mixing waveform. In the following section, we discuss several particular examples of the self-mixing measurements in semiconductor lasers.

11.2 Applications in Feedback Interferometer

11.2.1 Displacement and Vibration Measurement

In the signal processing system in Fig. 11.3, we obtain the number N of counted pulses as the output and the number is assumed to be large enough. Then, the displacement $\Delta L (L = L_0 + \Delta L$, L_0 being the offset length) of the external reflector is given by the following relation (Donati et al. 1996; Merlo and Donati 1997):

$$\Delta L = N\frac{\lambda}{2} + O(\lambda) \approx N\frac{\lambda}{2} \tag{11.5}$$

where $O(\lambda)$ is the residual of the counts. The direction of the displacement is determined from the total counted number of the up- and down-edges. Therefore, N has a plus or minus sign. Vibration measurement of an external reflector is also conducted by the same principle. For vibration measurement, the follow-up for time varying signals is important. When the time response of the signal processing circuits is fast enough, the measurement is limited by the response of the laser, i.e., the relaxation oscillation. Since the response of the laser is over nano-second, the total response of the measurement system with fast electronic circuits is up to nano-second. However, it is much faster than time variations of the ordinary mechanical vibrations we are considering.

The detection of a target displacement is the basic for interferometric measurement. We have shown an example of displacement measurement using self-mixing semiconductor lasers in the previous section. Here, we discuss vibration measurement in a self-mixing interferometer, which is the same principle as displacement measurement. When the amplitude of a target reflector under vibration is large enough (larger than the optical wavelength), we can obtain the frequency of the vibration from a

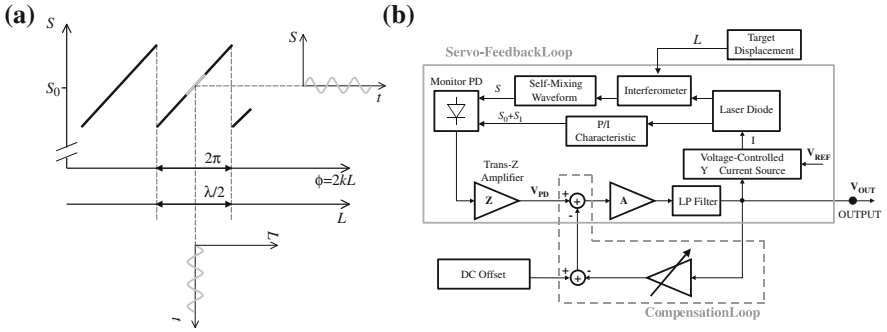

Fig. 11.5 **a** Principle of linear measurement of small target vibrations by locking the interferometer phase to half a fringe in the moderate feedback regime. The vertical axis represents the power emitted by the semiconductor laser, where S_0 is the power emitted by the unperturbed semiconductor laser. The horizontal axes represent interferometric phase and target displacement respectively. **b** Block diagram for the self-mixing vibrometer accomplishing the phase-locking and phase-nulling techniques. The details of input and output variables and each block are explained in the text [after Giuliani et al. (2003); © 2003 IOP]

Fourier transform analysis for the detected signal in the interferometer. Regardless of the optical feedback strength, the maximum frequency contained in the self-mixing signal for the case of a target vibrating at a frequency f_0 with amplitude ΔL is proportional to the product $f_0 \Delta L$. Indeed, a sinusoidal object vibration of 140 Hz frequency and 7.86 μm peak-to-peak amplitude is successfully measured by the method (Scalise 2002). However, only the product can be measured by the method, and we cannot obtain details of the vibration, such as the profile of the vibration amplitude.

To reconstruct a waveform of an object vibration, a closed loop technique is proposed. The principle of the measurement and the processing electronic circuits after the detection of a self-mixing signal are shown in Fig. 11.5 (Giuliani et al. 2003). At a moderate optical feedback of $C > 1$, we obtain a sawtooth-like interferometric signal as an output form the self-mixing in a semiconductor laser has already been discussed. Figure 11.5a shows the principle of linear measurement of small target vibrations by locking the interferometer phase to half a fringe in the moderate feedback regime, where the interferometric signal can be approximated as having a triangular shape. For a moment, we consider a small amplitude object vibration. At an operating offset intensity at S_0, the self-mixing output S is linearly proportional to the vibration amplitude and the waveform of the vibration is directly observed by an oscilloscope as far as the peak-to-peak amplitude of the object vibration is within $\lambda/2$.

By employing an additive active phase-tracking method, the maximum measurable vibration amplitude can be extended up to several hundred micron meters. The active phase-tracking system is designed so that a constant number of wavelengths are contained in the path from the semiconductor laser to the target. Figure 11.5b shows the block diagrams of the signal processing system. The blocks contained in the solid box constitute the servo-feedback loop and the blocks contained in the dashed box make up the compensation path. The main block is the self-mixing interferometer

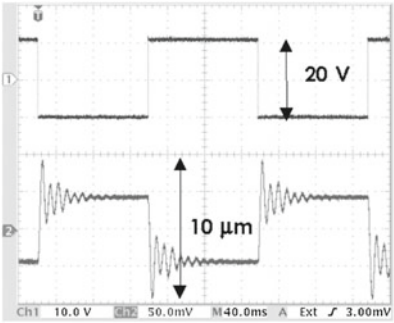

Fig. 11.6 Examples of vibration measurement. The target is a loudspeaker with a black paper surface driven by a 10 Hz square wave. *Upper traces*, loudspeaker drive signal, *lower traces*, vibrometer output signal [after Giuliani et al. (2003); © 2003 IOP]

operating in the moderate feedback regime, whose phase must be kept at a constant value, corresponding to half an interferometric fringe. The target displacement ΔL acts as a perturbation to the system, and it generates a variation $\Delta\phi$ of the interferometric phase. The phase variation $\Delta\phi$ causes a proportional variation ΔS in the power emitted by the laser through the self-mixing effect given by $\Delta S = \beta_{\mathrm{tr}}\Delta\phi$ (β_{tr} being the slope coefficient of the triangular transfer characteristics of the interferometer). The power variation is detected by the monitor photodiode and converted into the voltage signal ΔV_{PD} by the transimpedance amplifier, which is given by the relation as $\Delta V_{\mathrm{PD}} = \sigma Z \Delta S$ (σ is the net efficiency of the photodiode and Z is the trans-resistance). This signal is then amplified by a factor A, low-pass filtered, and fed to the input of the voltage-controlled laser current source with admittance Y, thus generating a variation I of the injection current as $\Delta I = AY\Delta V_{\mathrm{PD}}$. This, in turn, gives rise to a variation $\Delta\lambda$ of the laser wavelength such that $\Delta\lambda = \Delta I \cdot \mathrm{d}\lambda/\mathrm{d}I$. The feedback loop ensures that the phase variation generated by the laser wavelength variation is exactly opposite (at least at first order) to that caused by target displacement. The amplified error signal V_{OUT} fed to the current source is a perfect replica of the target displacement, and it constitutes the instrument output.

Figure 11.6 is an example of vibration measurements using the self-mixing vibrometer (Giuliani et al. 2003). The object is a loudspeaker driven by a square wave of 10 Hz. The semiconductor laser used is a commercial single-mode Fabry–Perot type with maximum power of 40 mW at the oscillation wavelength of 800 nm. The distance from the laser to the target is 80 cm. The amplitude of the vibration is much lager than $\lambda/2$, but we can obtain the full waveform of the oscillations as shown in the figure. As we can see, the damped resonance oscillations of the loudspeaker are clearly visible.

11.2.2 Absolute Position Measurement

When the injection current of a semiconductor laser is modulated, not only the laser output power, but also the oscillation frequency of the laser, change in accordance with the relation in (5.5). The same periodic undulation signal like in Fig. 11.2b or c

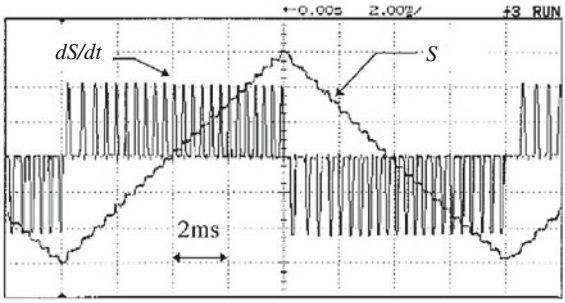

Fig. 11.7 Self-mixing signal for absolute distance measurement, obtained for a 0.8 mA current modulation in a Fabry–Perot semiconductor laser. The pulses are the analogue derivative of the laser output power, which corresponds the fringes to be counted for the distance measurement [after Giuliani et al. (2002); © 2002 IOP]

is observed for the laser output under the condition of the C parameter of $C \sim 1$ when a ramp signal is applied to the bias injection current of a semiconductor laser at a fixed external mirror position. The period of the undulations is equal to $c/2L$. For the measurement of the absolute position of a target (distance), a ramp signal, which has a linear increase or decrease for the time development, is usually used. By the ramp modulation, the oscillation frequency is also linearly changed. For a change of the injection current, the wavelength of the laser oscillation varies as $\Delta\lambda$, then the change of the wavenumber Δk is written by

$$\Delta k = -2\pi \frac{\Delta\lambda}{\lambda^2} = 2\pi \frac{\Delta\nu}{c} \tag{11.6}$$

where $\Delta\nu$ is the frequency change due to the injection current variation. For the reflecting mirror positioned at L from the laser facet, the change of the optical phase in the self-mixing interferometer due to the modulation is $\Delta\phi = \Delta k \cdot 2L$. The quantity of $\Delta\phi/2\pi$ is the number of interferometric fringes occurring from the wavelength variation $\Delta\lambda$ observed in the self-mixing interferometer, which is given by the following relation:

$$\frac{\Delta k \cdot 2L}{2\pi} = N + O(N) \tag{11.7}$$

Here, $O(N)$ represents the residual of fringe number, which corresponds to the maximum error in the distance measurement. By counting the number of fringes, one obtains the distance of the reflector from the laser facet, and the distance L is given by

$$L = \frac{\lambda^2}{2\Delta\lambda} N = \frac{c}{2\Delta\nu} N \tag{11.8}$$

Figure 11.7 shows the detected output power S of the laser swept by a ramp signal (Giuliani et al. 2002). Looking more closely, the signal resembles stepwise

variations of the output power, although the macroscopic change of the detected signal shows a linear increase or decrease for the time development. This step-wise change is induced by the selections of successive resonance external modes by the variation of the bias injection current for the laser; thus the output power shows not a smooth change but a step-wise change. The analogue derivative of the laser output power $\mathrm{d}S/\mathrm{d}t$ becomes a train of pulse-like signals, and this corresponds to the fringe signals discussed before. Counting the number of fringes for the duration of the ramp signal, we obtain the absolute distance with the relation in (11.8). The error in this measurement is the quantization error of fringes and the error corresponds to the maximum residual of the fringe counting in (11.7). Thus the maximum error is given by $c/2\Delta\nu$. Mourat et al. (2000) conducted the distance measurement using the self-mixing interferometer of a tunable multi-electrode DBR semiconductor laser having continuous tunable range up to 375 GHz and attained the accuracy of the measurement less than 0.5 mm for the distance of the order of meters. The accuracy is quite coincident with the theoretical resolution of $c/2\Delta\nu = 0.4$ mm.

11.2.3 Angle Measurement

Self-mixing interferometry is also applied for small angle measurement. In the angle measurement, coherence collapse states like in Fig. 11.2d is used (Giuliani et al. 2001). Figure 11.8 shows the experimental setup for small angle measurement in a self-mixing semiconductor laser. An external mirror under to test is tilted with a small angle θ_0 for the optical axis. In the optical setup, the direction of the illuminating light beam is changed by a reference mirror and the beam is directed to the reflector under the test. The feedback level is in regime IV and the laser output power shows coherence collapse states as shown in Fig. 11.2d when $\theta_0 = 0$. For a nonzero tilt angle, the feedback strength from the reflected light decreases with the increase of the tilt angle, but the reflected light is still fed back into the laser cavity and the tilt is such a small angle. In the measurement, the reference mirror put into the optical path is dithered with small amplitude of the tilt angle $\Delta\theta$. At the reference mirror angle for compensating the reflector tilt θ_0, the amount of the feedback light takes the maximum value. When the tilt of the reference mirror is a periodic function with time, the laser shows synchronous output with the modulation. However, the phase of the detected periodic function differs from that of the modulation due to the initial offset angle θ_0. Figure 11.9 shows the experimental results of the laser outputs in the angle measurement. In this figure, signal B corresponds to zero tilt of the external mirror and the output power includes the second harmonic component due to rather strong optical feedback. However, the initial phases of signals A and C are shifted from that of the driving signal and the small angles are calculated from the phase shifts. The tilt angle of the external mirror has a linear relation with the detected phase shifts for a certain range of the tilt. In this technique, we need some calibration for a particular setup of the experiment. We can perform a small tilt angle detection on the order of 10^{-6}–10^{-4} rad based on this technique.

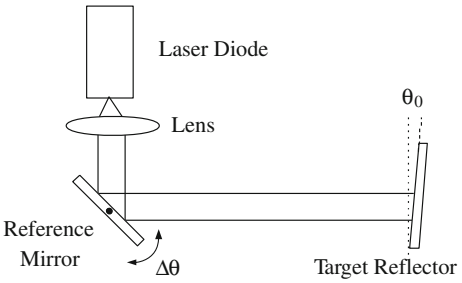

Fig. 11.8 Experimental setup for angle measurement in a self-mixing semiconductor laser. The external mirror under test is tilted with a small angle θ_0. The reference mirror is dithered with a small amplitude

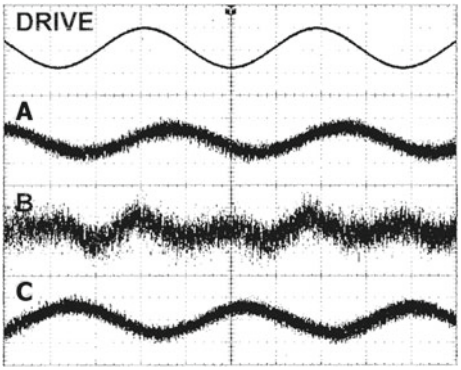

Fig. 11.9 Waveforms of self-mixing laser outputs. *Upper trace*: drive signal of a reference mirror. Laser output powers **A**: with negative tilt, **B**: zero tilt, and **C**: positive tilt. The frequency of the driving signal is 180 Hz [after Giuliani et al. (2001); © 2001 SPIE]

11.2.4 Measurement of the Linewidth Enhancement Factor

The linewidth enhancement factor α of a semiconductor laser is an important parameter for deciding its dynamical characteristics. As discussed in Chap. 3, the real and imaginary parts of the complex susceptibility in semiconductor lasers are not determined independently, but they have a certain relation. This fact gives rise to the nonzero finite value of the linewidth enhancement factor. For most lasers such as gas lasers, the value of the linewidth enhancement factor α is zero, while it has a value around $\alpha = 3 - 7$ in semiconductor lasers (see Sect. 3.3.3). As a result, the linewidth of the laser oscillation is broadened by as much as several tens of MHz to 100 MHz. On the other hand, for lasers with a linewidth enhancement factor of $\alpha = 0$, the linewidth is usually less than MHz as discussed in Chap. 3. There are several methods to measure the factor (Okoshi et al. 1980). It is also measured by analyzing the laser output power for a sinusoidal modulation of the external mirror position in a self-mixing interferometer. For a certain range of optical feedback strength of an external reflector, a periodic sawtooth-like wave is observed for the change of the external cavity length in the laser output power. We can measure the linewidth enhancement factor from jitters of the sawtooth-like waves.

We assume that the oscillation frequency of a semiconductor laser is $\nu = \nu_0 + \delta\nu$, where $\delta\nu$ is the fluctuation of the laser oscillation. In the measurement of the linewidth

enhancement factor, the position of the external mirror is modulated by a sinusoidal signal and the external mirror is vibrated with a small amplitude compatible with the order of the optical wavelength. Using the modulation for the external mirror position $l_m(t)$ with zero mean and putting the external cavity length $L = L_0 + l_m(t)$, the back-reflected field phase is given by

$$\phi = \frac{4\pi}{c}\nu L = \frac{4\pi}{c}\nu_0 L + \frac{4\pi}{c}\nu_0 l_m(t) + \frac{4\pi}{c}\delta\nu L \tag{11.9}$$

The phase ϕ is a periodic function with period $\lambda/2$, but it is a statistical function due to random fluctuation of $\delta\nu$.

On averaging the phase and its square and calculating the covariance, the statistical root-mean-square (rms) phase related to the linewidth enhancement factor is given by (Giuliani and Norgia 2000)

$$\sqrt{\langle(\Delta\phi)^2\rangle} = \sqrt{\langle\phi^2\rangle - \langle\phi\rangle^2} = \frac{4\pi}{c}L_0\overline{\delta\nu} \tag{11.10}$$

where $\overline{\delta\nu}$ is the average of the frequency fluctuations. The average $\overline{\delta\nu}$ is equal to the laser linewidth $\Delta\nu$ in (3.114), which gives the relation between the phase fluctuation and the linewidth enhancement factor α. Figure 11.10 shows the experimental result of jitter in the measurement of linewidth enhancement factor. Figure 11.10a shows the driving signal for the position of the external mirror and the periodic output power. Figure 11.10b shows the zoomed frame with the superposition of subsequent single-sweep acquisitions of the self-mixing signal. The periodic signal contains detailed structures and there is jitter in up- or down-edges of the sawtooth-like wave in the laser output power. From the statistical average of the jitters, the relation between the rms phase and the linewidth enhancement factor is calculated according to (11.10). In the real experiment, the measurement is repeatedly conducted for different absolute positions of the external mirror and the value of $4\pi\delta\nu_0/c$ is obtained as the proportional coefficient. The amount of feedback required to achieve the self-mixing regime is moderate (i.e., around 10^{-6} in power), so that the optical feedback little affects the linewidth of the laser oscillations and the linewidth measured under the small perturbations remains almost the same value as the solitary oscillations.

The linewidth enhancement factor can also be obtained by the above same optical system by calculating two-phase separations; one is the separation between a zero-crossing phase of the approaching signal and the phase at the adjacent down-edge, and the other is the separation between a zero-crossing phase of the leaving signal and the phase at the adjacent up-edge. Form the comparison between the two-phase values, the linewidth enhancement factor can be calculated either graphically or numerically (Yu et al. 2004). The values of the linewidth enhancement factor from 2.2 to 4.9 are experimentally obtained for various different lasers with different oscillation wavelength. The values of the linewidth enhancement factor measured using the proposed technique are in good agreement with those obtained by using the self-heterodyne method (Okoshi et al. 1980). It is finally noted that, as pointed

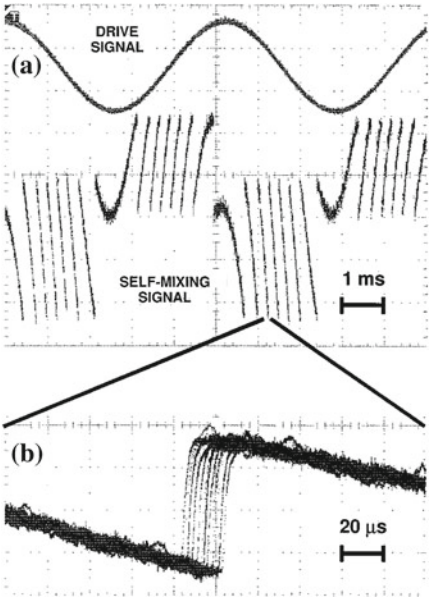

Fig. 11.10 Measurement of linewidth enhancement factor. **a** Driving signal of the external mirror position (*upper trace*, 1 V/div corresponding to 1.43 μm/div target displacement) and corresponding laser output (*lower trace*, 1 ms/div time scale) in self-mixing interferometer. **b** Zoomed frame of superposition of subsequent single-sweep acquisitions of signal. The time scale of 20 μs/div corresponds to the phase variation of 0.5 rad/div [after Giuliani and Norgia (2000); © 2000 IEEE]

out in Sect. 8.7.2, self-mixing effects are suited for the measurement of the linewidth enhancement factor in quantum-cascade semiconductor lasers for the lack of compact and sensitive detectors in the THz band.

11.3 Self-Mixing Doppler Velocimetry

11.3.1 Velocity Measurement

For a continuous movement of an external reflector, the output power from the laser by self-mixing exhibits a Doppler beat signal. The field rate equation for such a continuous movement as a function of time t needs to be modified for practical numerical simulations. Velocity measurement is considered as a continuous change of the external mirror position, however, as discussed in the previous section, it can be easily analyzed by the extension of the displacement measurement as the first approximation. When the external mirror moves, the detected signal changes as $\Delta S = \Delta S_0 \cos \omega_s \tau$ in accordance with (11.3). The external cavity roundtrip time τ is a time dependent function and is proportional to the external cavity length L. Considering the angle θ of the motion for the optical axis, the round trip time τ is written by (Bosch et al. 2001)

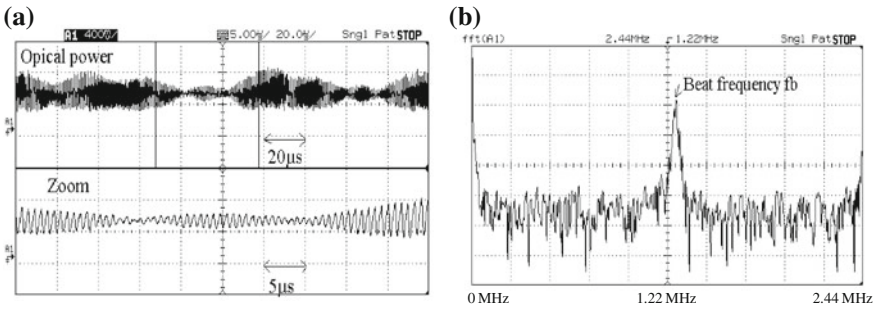

Fig. 11.11 Example of velocity measurements using self-mixing semiconductor laser. **a** Time-domain self-mixing signal for velocity measurement on a rotating diffusing target. **b** FFT spectrum of the signal. The Doppler beat frequency 1.46 MHz corresponds to a speed of 0.56 m/s [after Giuliani et al. (2002); © 2002 IOP]

$$\tau(t) = \frac{2}{c}(L_0 \pm vt\cos\theta) \tag{11.11}$$

where v is the speed of the external mirror and L_0 is the offset distance of the reflector from the laser facet at $t = 0$. The signs of the velocity term account for the direction of the motion; the plus sign is for the object moving away from the laser and the minus sign is for moving toward the laser. The self-mixing in semiconductor lasers is of the heterodyne detection and the term related to the velocity in (11.11) corresponds to a Doppler shift component in the self-mixing (Groot and Gaillatin 1989; Shinohara et al. 1989; Aoshima and Ohtsubo 1992). As has already been discussed in the displacement measurement, we can discriminate the direction of the movement from the shape of waveforms of the self-mixing signal. Two-dimensional velocity measurement is easily implemented by extending the 1D measurement.

Figure 11.11 shows an experimental self-mixing signal in time-domain from a rough rotating disc with a small feedback fraction $C < 1$ (Giuliani et al. 2002). In Fig. 11.11a, the self-mixing amplitude is strongly deformed by speckle modulation compared with a flat reflecting surface. Therefore, it may be difficult to extract the velocity information from the time signal by the fringe counting technique, as done in the displacement measurement. However, the harmonic component corresponding to the disc velocity is easily obtained from the Fourier spectrum as shown in Fig. 11.11b, although the spectrum has a broadened peak due to the speckle effect. Using the technique of the self-mixing in semiconductor lasers, velocity measurements ranging from a rigid surface of ∼100 m/s to a slow blood flow of ∼mm/s have been performed (Özdemir et al. 2000; Giuliani et al. 2002).

11.3.2 Rigorous Rate Equations of Self-Mixing Doppler Effects

As mentioned in the previous subsection, the field equation in the presence of time-dependent continuous change of the external mirror must be modified from (4.2) in a static optical feedback case. As a first step to derive the rigorous equation of optical feedback for a continuously moving reflector, we derive the form of the feedback field in the presence of the Doppler effect. At the exit facet of the laser, the complex field of the feedback light including optical frequency oscillations, $\hat{E}_{\text{feedback}}(t)$, from a moving reflector with a constant vector velocity $\mathbf{v}$ is given by the following equation (Durst et al. 1976):

$$\hat{E}_{\text{feedback}}(t) = E(t-\tau)\exp[i(\mathbf{k}_i \cdot \mathbf{r}_i + \mathbf{k}_s \cdot \mathbf{r}_s) - i\omega_0 t] \tag{11.12}$$

where $\mathbf{k}_i$ and $\mathbf{k}_s$ are the vector wavenumbers to and from the reflector at time t, $\mathbf{r}_i$, and $\mathbf{r}_s$ are the accompanying position vector coordinates, and ω_0 is the angular frequency of the internal laser oscillation. The equation is for a single optical feedback and is valid for a weak optical reflection. We apply the relations $\mathbf{r}_i = \mathbf{r}_i' + \mathbf{v}t$, $\mathbf{r}_s = \mathbf{r}_s' - \mathbf{v}t$, $\mathbf{k}_i \approx \mathbf{k}_i'$, $\mathbf{k}_s \approx \mathbf{k}_s'$, $\mathbf{k}_s = -\mathbf{k}_i$, $\mathbf{r}_s = -\mathbf{r}_i$, $\mathbf{r}_s' = -\mathbf{r}_i'$, and $|\mathbf{k}_i| = |\mathbf{k}_s| = k = \omega_0/c$, where $\mathbf{r}'$ and $\mathbf{k}'$ correspond to respective variables at time $t = 0$. Then the complex field is written as

$$\hat{E}_{\text{feedback}}(t) = E(t-\tau)\exp[i\omega_0\tau_0 - i(\omega_0 - \omega_d)t] \tag{11.13}$$

where τ_0 is the offset round trip time of light $\tau_0 = 2L_0/c$ and ω_d is the Doppler shifted angular frequency $\omega_d = 2\pi\nu_d = 2\omega_0 v/c$. τ is the round trip time of light scattered from the moving object and is written as

$$\tau = \frac{\mathbf{r}_i - \mathbf{r}_s}{c} = \frac{2}{c}(L_0 + vt) \tag{11.14}$$

Here, the expression is the same as (11.11), however, we assume that $\theta = 0$ and the plus or minus sign is included in the parameter v depending on whether the reflector is approaching to or leaving from the front facet of the laser. Since the round trip time τ is a function of time t, it is difficult to directly perform numerical calculations simply applying the feedback field of (11.13) into (4.2).

Substituting (11.14) into (11.13), the delay field is explicitly written by

$$E(t-\tau) = E\left(t - \tau_0 - \frac{2v}{c}t\right) = E[a(t-\tau_0')] \tag{11.15}$$

where $a = 1 - 2v/c$ and $\tau_0' = \tau_0/a$. Since the velocity of interest is much smaller than the speed of light $v \gg c$ and, thus, a is very close to unity, τ_0' is approximated as

$$\tau_0' \approx \tau_0\left(1 + \frac{2v}{c}\right) \tag{11.16}$$

Therefore, the feedback field has a time scale, at, different from the original field $E(t)$. To adjust different time scales within the same differential equation, the method of Mellin transform is effective. A function of t, $E[(1-\varepsilon)t]$ with a small value of ε can be expanded as a non-scaled function $E(t)$ by virtue of the Mellin transform (Gradshteyn and Ryzhik 1980). Then the function $E[(1-\varepsilon)t]$ is approximated as

$$E[(1-\varepsilon)t] \approx E(x) - \varepsilon t \frac{\mathrm{d}E(t)}{\mathrm{d}t} \tag{11.17}$$

Note that the above equation looks like a simple approximation as a Taylor series expansion. However, the result is not self-evident, since $E[(1-\varepsilon)t]$ is a function of a scaled variable. Putting $a = 1-\varepsilon$ and replacing t as $t - \tau_0'$, the delay differential field equation for Doppler self-mixing is finally given by (Ohtsubo et al. 2009):

$$\begin{aligned}\frac{\mathrm{d}E(t)}{\mathrm{d}t} &= \frac{1}{2}[(1-i\alpha)G_n[n(t)-n_{\mathrm{th}}]E(t) \\ &\quad + \frac{\kappa}{\tau_{\mathrm{in}}}\left[E(t-\tau_0') - \frac{2v}{c}(t-\tau_0')\frac{\mathrm{d}E(t-\tau_0')}{\mathrm{d}t}\right]\exp[i(\omega_0\tau_0 + \omega_d t)]\end{aligned} \tag{11.18}$$

Using (11.18), we can perform numerical calculations not only for periodic beating signal but also for chaotic oscillations in the presence of continuous time-dependent external mirror movement. For the carrier density n, which is the counterpart variable for calculating the dynamics in self-mixing semiconductor lasers, the same equation as that for optical feedback from a fixed reflector can be used.

Figure 11.12 shows numerical examples of time series of Doppler shifted waveform. The offset position of the external reflector is $L_0 = 9\,\mathrm{cm}$ and the laser is biased at $J = 1.3J_{\mathrm{th}}$. The other parameter values used are almost the same as those in Table 5.1. Therefore, the chaotic bifurcation diagram is the same as that in Fig. 5.7a and the laser evolves into chaotic oscillations through like a Hopf bifurcation. As the external reflectivity increases, the output power of the self-mixing semiconductor laser shows sinusoidal oscillations in Fig. 11.12a and sawtooth-like periodic oscillations in Fig. 11.12b. The Doppler frequency is $v_d = 2.55\,\mathrm{MHz}$ (equivalent to a time period of 391.5 ns). Over a certain breaking point, the laser becomes unstable and oscillates with a burst-like waveform as shown in Fig. 11.12c. While Fig. 11.12c does not show it clearly, the frequency of the periodic burst corresponds to the relaxation oscillation. Even for such unstable oscillations, the Doppler frequency is still visible in the waveform. In Fig. 11.12d, the main Doppler frequency is still preserved, but the laser becomes less stable. If we replace the time scale with an external cavity length, very similar waveforms as those shown in Fig. 11.12a, b are observed for static optical feedback for a discrete change in the mirror position. However, different dynamics are observed for a range of intermediate optical feedback ratios, which are not observed for a static displacement. For moderate optical feedback, the periodicity of the Doppler effect is barely detectable, as shown in Fig. 11.12e. However, with

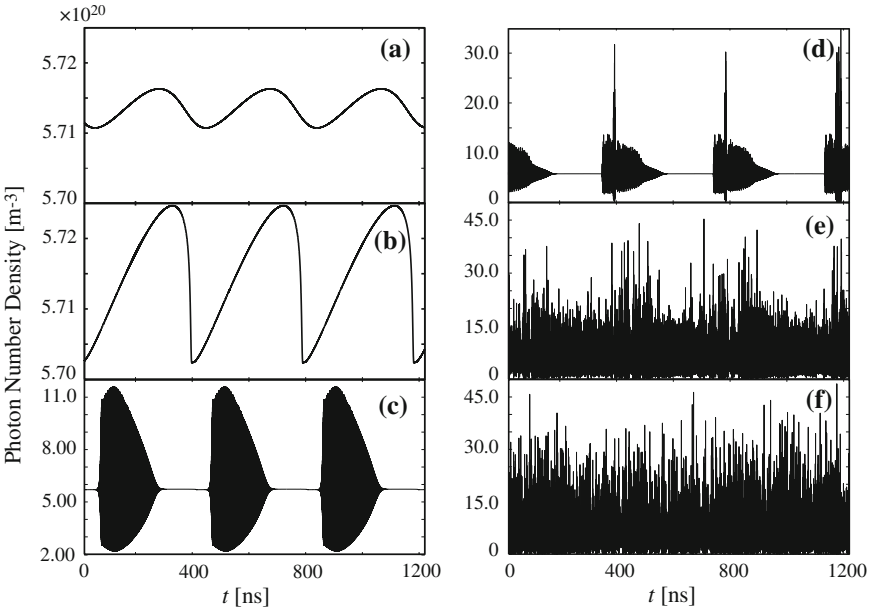

Fig. 11.12 Time series of Doppler-shifted waveform (photon number density) for variations of external mirror reflectivities. **a** $r = 0.000402$, **b** $r = 0.00161$, **c** $r = 0.00241$, **d** $r = 0.0109$, **e** $r = 0.0153$, **f** $r = 0.0233$. The offset position of the external reflector is $L_0 = 9\,\text{cm}$ and the laser is biased at $J = 1.3 J_{\text{th}}$. The parameter values almost similar to those listed in Table 5.1 are used for the numerical simulations

a further increase in the external reflectivity in Fig. 11.12f, the laser output shows completely chaotic oscillation and no Doppler frequency component is observed in the waveform.

11.4 Chaotic Lidar

For an optical remote sensing technology, LIDAR (Light Detection And Ranging, or it is sometimes called Laser Rader), that can measure the distance or the properties of a target, has been developed since 1970. In this technique, either short-pulses or random pulse sequences modulated by microwave range is used as a source for illuminating a target. In the common short-pulse technique, the time of flight is measured directly and the range resolution, which is determined by the pulse width, is typically in the range of meters. As an alternative technique, pseudorandom code-modulated CW lidar has been developed. In this technique, target detection and localization are accomplished either by correlating the signal waveform reflected or backscattered from the target with the time-delayed reference waveform or by interfering them optically with a Michelson interferometer, where the range resolution is determined by

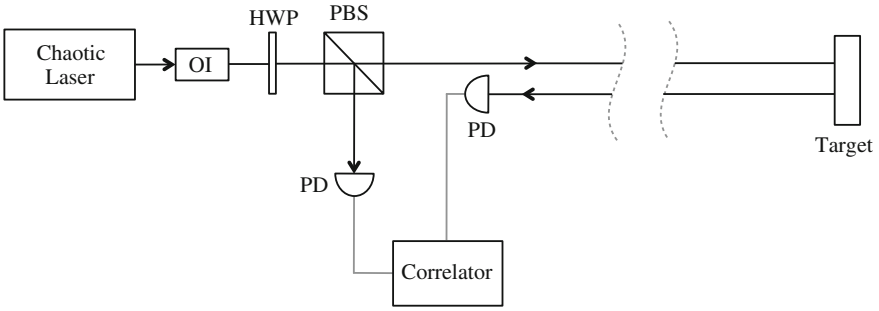

Fig. 11.13 Schematic setup of chaotic lider. OI: optical isolator, HWP: half-wave plate, PBS: polarization beam splitter, PD: photodetector

the bandwidth of the modulated waveform. Based on this technique, higher resolution that measured by short-pulse light sources is attained up to 5 cm. Instead of random modulation, chaotic lidar has been proposed (Lin and Liu 2004a,b). As discussed in this book, chaos in semiconductor lasers exhibits very high-speed oscillations and has very broad bandwidth with flat spectral profile in microwave region. Therefore, it is very suited for a light source of lidar. Further, compared with conventional radars, chaotic lidar has the advantages of very high-range resolution, unambiguous correlation profile, possibility of secure detection, low probability of intercept, and high electromagnetic compatibility. The needs of high-speed random-code generation and modulation electronics no longer exist and the ambiguity caused by the limited length of pseudorandom codes or a repeated waveform is also eliminated because a chaotic waveform never repeats itself. One of promising applications similar to chaotic lidar is a chaotic correlation optical time-domain reflectometer (CC-OTDR). Wang et al. (2008) successfully demonstrated an OTDR for measuring the distribution of the reflectivity along an optical fiber transmission line based on the chaotic correlation technique by experiment. In the following, we will discuss the principle of chaotic lidar and its performance.

Figure 11.13 shows a schematic setup of a chaotic lidar. The light source is a high-speed chaotic semiconductor laser. Chaotic oscillations in semiconductor lasers are generated by for examples, optical injection, optical feedback, or optoelectronic feedback. An optical isolator is placed right after the chaotic laser to prevent unwanted optical feedback. The chaotic output is split by a polarizing beam splitter into two beams, one serving as the probe beam and the other as the reference. By rotating the angle of the half-wave plate relative to the polarizing beam splitter, the power ratio between these two beams can be adjusted. The probe beam is directed to the target, and the signal light that is backscattered or reflected from the target. In a practical field application, high power semiconductor laser is used as a light source and telescope transmitter and receiver are used to transmit and detect chaotic signals. The signal is collected and detected by a combination of lens and detector. The detection and ranging are realized by correlating the signal waveform reflected back from the

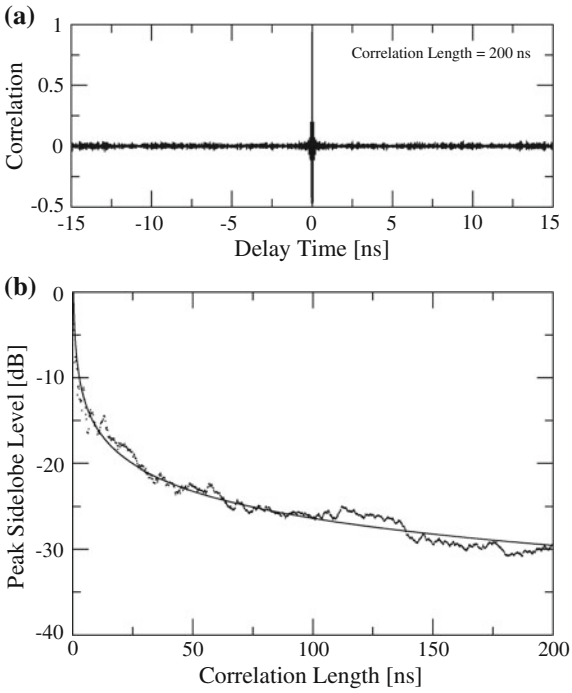

Fig. 11.14 **a** Numerical example of autocorrelation for a chaotic oscillation generated by optical injection. **b** Peak side-lobe level versus correlation length. The solid line is the regression. To generate chaos in the semiconductor laser, optical injection is used. The injection strength is 0.046 (amplitude) and the frequency detuning between the injected and slave lasers is 0 GHz [after Lin and Liu (2004a); © 2004 IEEE]

target with a delayed reference waveform. The performance of the lidar is mainly determined by the generated chaotic state. To have a δ-function-like correlation trace that has a highest possible resolution and lowest possible detection ambiguity, chaotic lidar should be operated in a state that its chaotic waveform has similar properties to those of white noise, such as a flat, smooth, and broad spectrum more than 10 GHz, and a noise-like time series. Chaotic lidar has a much higher range resolution benefiting from the broad bandwidth of the optical chaos. Indeed, due to the very broad bandwidth of the chaotic waveform that can be easily generated by a semiconductor laser, a centimeter-range resolution is readily achieved.

Figure 11.14a shows a numerical example of autocorrelation traces of the time series of generated chaotic light with a correlation length of 200 ns (Lin and Liu 2004a). The chaotic oscillations generated by optical injection to a semiconductor laser with the injection strength of 0.046 in amplitude and the frequency detuning of 0 GHz between the master and slave lasers at the bias injection current of $2J_{\mathrm{th}}$. The laser has a free-running relaxation frequency of 12 GHz at this bias injection current. A narrow correlation spike without any apparent side-lobe is visible and its full-width at half-maximum (FWHM) of the spike, namely, the range resolution, is 0.9 cm, which is much higher than the resolution of a conventional radar. To quantify the performance in a radar system, the peak side-lobe level (PSL) is frequently used. Peak side-lobe level is defined as the ratio of the maximum side-lobe to the peak; it is associated with the probability of a false signal in a particular range bin due to

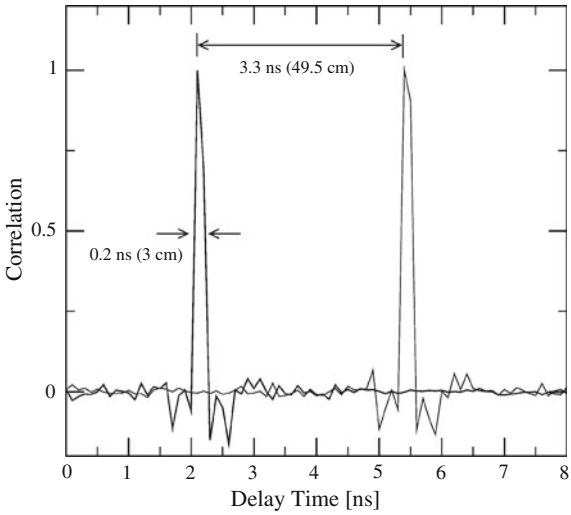

Fig. 11.15 Cross-correlation traces of a target moving about 50 cm in the line of sight [after Lin and Liu (2004b); © 2004 IEEE]

the presence of a target in a neighboring range bin. The peak side-lobe level for the chaotic signal is shown for the correlation length in Fig. 11.14b. The peak side-lobe level for the chaotic signal shows a better correlation performance than those of any other lidar systems. Thus, the chaotic waveform generated by an optically injected semiconductor has superior characteristics for radar applications without the need of any sophisticated microwave circuit.

To demonstrate the feasibility of chaotic lidar, a laboratory experiments were carried out (Lin and Liu 2004b). Figure 11.15 shows the result of cross-correlation obtained by a target moving about 50 cm in the line of sight. The laser used is a single-mode distributed feedback InGaAsP/InP semiconductor laser with a wavelength of 1.3 μm. Chaotic oscillations are generated by optical injection under appropriate conditions of the optical injection and the frequency detuning, and the bandwidth of the chaotic signal is measured to be more than 15 GHz. The target mirror is arranged at about 2 m away from the chaotic lidar system on a translation stage. A set of signal and reference waveforms are first obtained and the cross-correlation trace of them is plotted in Fig. 11.15 (the curve corresponds to a correlation peak at 2.1 ns). By translating the mirror about 50 cm away in the line of sight, a second set of signal and reference waveforms are obtained, and their cross-correlation trace is plotted (the curve corresponds to a correlation peak at 5.4 ns). In both cases, the correlation lengths are 2 μs. From the separation between the correlation peaks, the relative range difference is measured to be 49.5 cm showing a sub-centimeter accuracy in ranging. A 3-cm range resolution is achieved with a 0.2-ns FWHM of the cross-correlation peak. However, the resolution is not the limitation for the essential system but the limitation for the equipment used in the experiment. The peak side-lobe level is calculated to be 27 dB and the signal-to-noise ratio of 27.5 dB is obtained in this

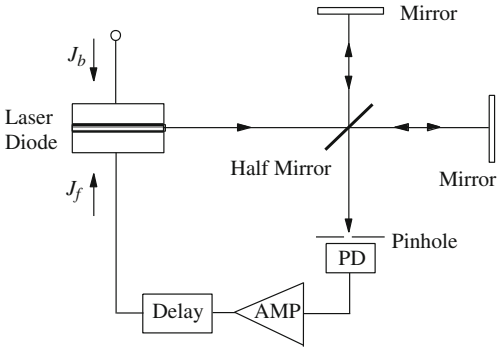

Fig. 11.16 Model of Twyman-Green active feedback interferometer. The fringe of the interferometer output is detected by a photodetector (PD) through a pinhole smaller than the fringe spacing

experiment. The chaotic lidar system has an excellent performance in correlation such that target detection can be done unambiguously with a very high resolution.

11.5 Active Feedback Interferometer and Applications

11.5.1 Stability and Bistability in Active Feedback Interferometer

Another type of feedback interferometer is a system of a two-arm interferometer with optoelectronic feedback. Here, we discuss the feedback of the interference light to the bias injection current of a semiconductor laser. Such a system is considered as a kind of filtered feedback systems discussed in Sect. 4.7. For example, in a Twyman-Green interferometer, the optoelectronic feedback technique is applied to stabilize the fringe of the interferometer output from disturbances such as mechanical vibrations. Such a system opens wide applications for the fringe analysis and measurements of laser interferometer under various circumstances of the atmosphere (Yoshino et al. 1987). Figure 11.16 is an example of laser interferometers with optoelectronic feedback. The interferometer output is detected by a photodetector through a small pinhole. The diameter of the pinhole is assumed to be much smaller than the fringe spacing. The detected photocurrent is fed back to the bias injection current of the light source of the semiconductor laser. The principle of the stabilization of the interferometer is as follows; the detected optical power deviates when the fringe is disturbed by the external perturbation. Then, the detected photocurrent changes and the injection current to the laser is modulated. The change of the laser output power induces the optical frequency change so as to compensate and cancel the fluctuations of the fringe intensity at the detection point. The variation of the optical frequency is at most several GHz in ordinary feedback interferometers. We can ignore the effect of disturbance by the optical frequency change on the accuracy of the interferometric measurement, since the ratio of the change to the center optical frequency is only less than 10^{-5}. However, care must be taken with respect to the feedback strength.

In this active interferometer, stability, multistability, and chaos appear in the laser output depending on the feedback strength and the response time of the feedback loop. In the following, we discuss the principle and behaviors of the active feedback interferometer, and applications for chaos control and signal generations.

We have investigated the effects of optoelectronic feedback in semiconductor lasers in Chap. 7. A similar treatment can be applied to the active interferometer, but the feedback signal is an interference fringe. The rate equations we use are

$$\frac{\mathrm{d}S(t)}{\mathrm{d}t} = G_n\{n(t) - n_{\mathrm{th}}\}S(t) + R_{\mathrm{sp}} \tag{11.19}$$

$$\frac{\mathrm{d}n(t)}{\mathrm{d}t} = \frac{1}{ed}\{J - \xi x(t)\} - \frac{n(t)}{\tau_s} - G_n\{n(t) - n_0\}S(t) \tag{11.20}$$

where $x(t)$ is the term of optoelectronic feedback. As discussed in Chap. 7, the electronic feedback circuit usually has a finite time response and the variable $x(t)$ follows a differential equation similar to (7.8). Here, we write the response of the feedback term as follows:

$$\tau_i \frac{\mathrm{d}x(t)}{\mathrm{d}t} = -x(t) + \frac{J_f(t)}{\xi} \tag{11.21}$$

where τ_i is again the response time of the electric circuit and J_f is the feedback current to the bias injection current. $x(t)$ is the variable of the feedback and it corresponds to the photon number as a physical quantity. Therefore, ξ is the conversion efficiency from the current density to the photon number. The feedback current of the active interferometer is easily calculated as (Ohtsubo and Liu 1990; Liu and Ohtsubo 1992a,b)

$$J_f(t) = \xi x_b - G_A \xi x(t)[1 + b\cos\{\kappa_i x(t) - \phi_0\}] \tag{11.22}$$

where x_b is the reference signal in the feedback circuit and G_A is the gain of the circuit. The cosine term on the right-hand side of (11.22) denotes the fringe in the interferometer output and b is the visibility of the fringe. ϕ_0 is an offset phase in the interferometer. The laser frequency is changed by the feedback current. The cosine term in (11.22) is the effect of the frequency change. Using the optical frequency ν_0 without feedback, the frequency $\nu(t)$ in the presence of feedback is written by $\nu(t) = \nu_0 - \beta_f x(t)$. Then, the argument of the cosine function reads

$$-\kappa_i x(t) + \phi_0 = -\frac{4\pi D_i \nu(t)}{c} = -\frac{4\pi D_i \beta_f}{c} x(t) + \frac{4\pi D_i \nu_0}{c} \tag{11.23}$$

where D_i is the difference of the interferometer arms and β_f is the conversion efficiency from the photon number to the oscillation frequency in the semiconductor laser.

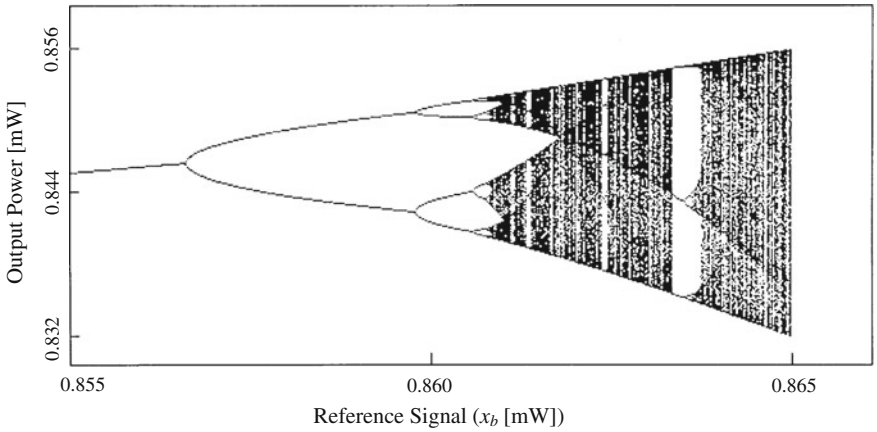

Fig. 11.17 Bifurcation diagram of laser output in active delay feedback interferometer for change of bias injection current. The parameters are $G_A = 0.05$, $\kappa_i = 32\pi$, and $\phi_0 = 0$

If the responses of the electronic circuits and the laser are much faster than the time-varying external disturbances for the interferometer, only (11.22) is sufficient to describe the system characteristics of the active interferometer. We here discuss the stability and instability of the system when the response time of the feedback circuit is fast enough, $\tau_i \sim 0$. Indeed, possible mechanical vibrations for the interferometer are less than 1 kHz. Therefore, solutions of stability, bistability, and multistability of the laser output are investigated from the crossing points for the graph of $y = x(t)$ and $y = J_f(t)$ in (11.22). When the disturbance for the interferometer is small enough, we can obtain a stable solution of the interferometer. In this active interferometer, the configuration of the imbalance interferometer is essential, since the feedback signal depends on the difference according to (11.23). The interferometer is always stabilized at a certain fringe pattern as far as the deviation or distortion of the fringe pattern by the disturbance is smaller than the fringe separation. Thus, we can attain robust interferometric measurement under unfavorable conditions of disturbances and the fringe analysis is performed under such severe conditions. When the disturbance is large enough with exceeding the fringe spacing, multi-stable states appear in the laser output and hops of the optical frequency through the feedback are induced. This gives rise to chaotic behaviors in the laser output (Ohtsubo and Liu 1990; Liu 1994). The technique of the active interferometer cannot be applied for the phase scanning interferometer, since the phase shift of the fringe is an essential technique in the phase scanning interferometry.

The active interferometer shows rich varieties of dynamics when the feedback circuit has a time delay. By the introduction of the delay, the system exhibits stability, instability, and chaotic states depending on the feedback delay and ratio. We here consider the following modified equation for (11.23) for the delayed system (Liu and Ohtsubo 1992a,b):

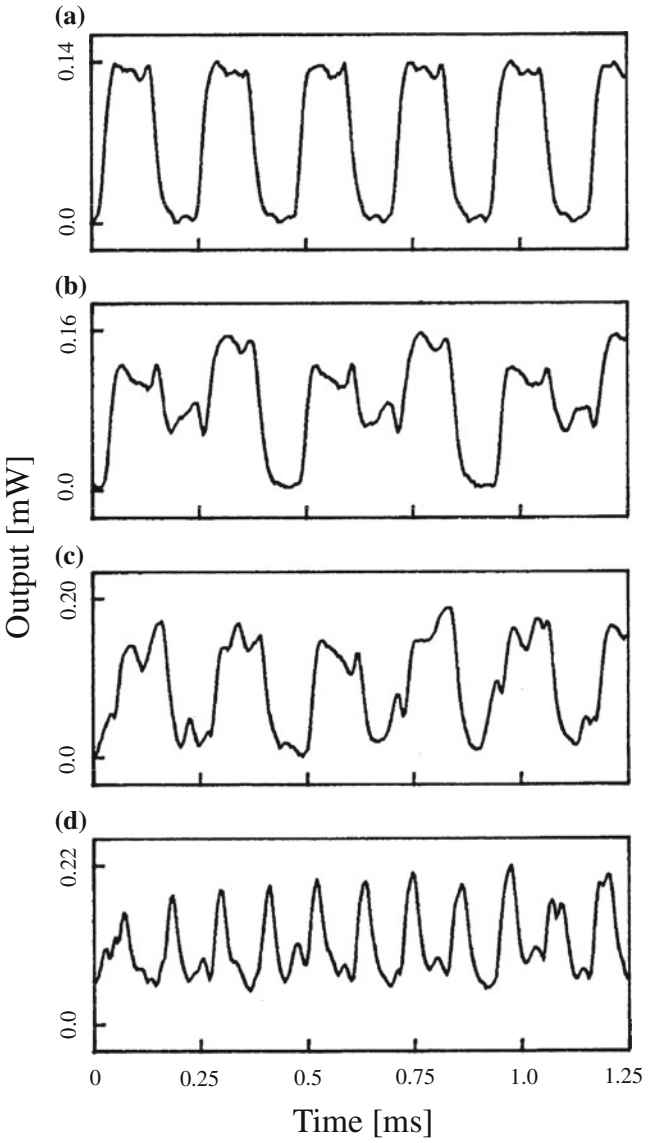

Fig. 11.18 Chaotic oscillations in an active delayed feedback interferometer at $G_A = 0.05$, $\kappa_i = 32\pi$, $\phi_0 = 0$, and $\tau = 0.1$ms. **a** $x_b = 0.423$mW with period-1 state, **b** $x_b = 0.30$mW with period-4 state, **c** $x_b = 0.473$mW with period-1 chaos, and **d** $x_b = 0.573$mW with fully developed chaos

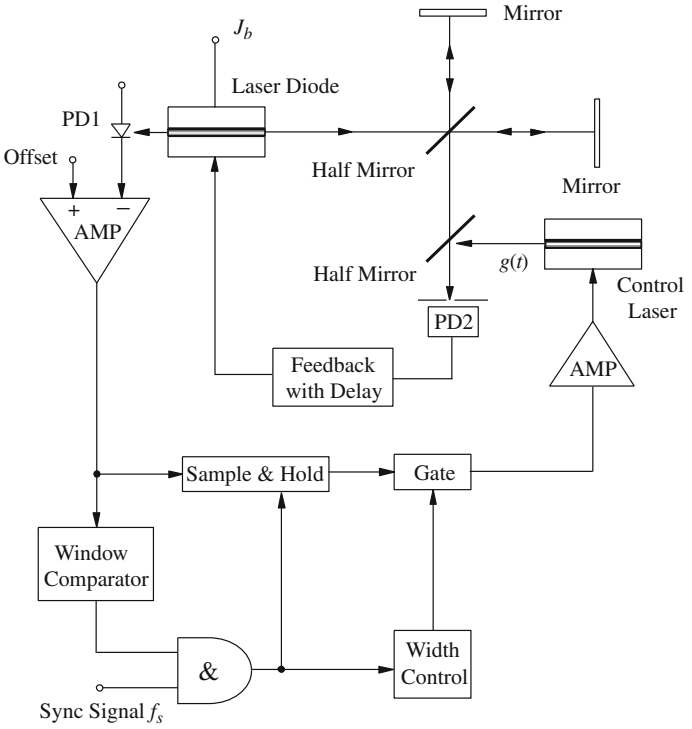

Fig. 11.19 OPF control for chaotic oscillations in an active delay feedback interferometer

$$J_f(t) = \xi x_b - G_A \xi x(t - \tau_e)[1 + b\cos\{\kappa_i x(t - \tau_e) - \phi_0\}] \tag{11.24}$$

where τ_e is the delay time in the feedback circuit. Figure 11.17 shows the calculated bifurcation diagram of the laser output for the change of the reference signal (the bias injection current). The bifurcation diagram is obtained by assuming the difference equation described by (11.24) instead of solving the continuous rate equations. The laser output clearly shows typical chaotic evolution via period doubling bifurcation. Figure 11.18 shows experimentally obtained waveforms in the active interferometer for the change of reference signal level. With increasing the reference signal level, the laser output evolves from a periodic oscillation into chaotic states. The period $2T$ of the period-1 oscillation in Fig. 11.17a is about $2T = 0.22$ ms and it is almost equal twice the delay time of the circuit of $\tau_e = 0.10$ ms. The difference of time $T - \tau_e = 0.01$ ms is equal to the intrinsic delay τ_i of the whole circuit except for the extra delay circuit. In this chaotic system, we can easily design periodic orbits by appropriately choosing the system parameters and generate arbitrary waveform sequences in the laser output prior to chaotic states. These higher harmonic oscillations are used for the applications of chaotic associative memory (Liu and Ohtsubo 1992b, 1993, 1994b).

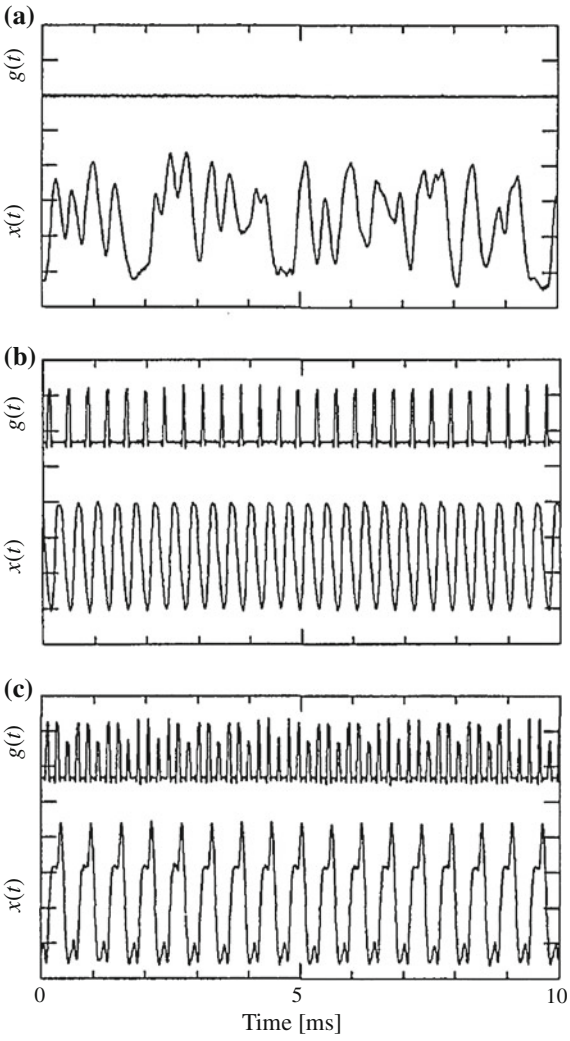

Fig. 11.20 Experimental results of chaos control in an active delay feedback interferometer. **a** Chaotic oscillation without control. **b** 11th harmonics of fundamental period-1 orbit with control (synchronous frequency is 2.64 kHz). **c** 7th harmonic oscillation of fundamental period-1 orbit with control (synchronous frequency is 5.04 kHz). The delay time of the circuit is $\tau_e = 2.0$ ms. *Upper trace* of each figure is the control signal $g(t)$ (arbitrary amplitude) and *lower trace* is the controlled waveform $x(t)$

11.5.2 Chaos Control in Active Feedback Interferometers

Chaotic oscillations in active delayed feedback interferometers can be also controlled to periodic or fixed states based on the chaos control method. In this subsection, we describe chaos control in the active interferometer by the occasional proportional feedback (OPF) method. The active feedback interferometer was originally designed for the isolation of rather slow response mechanical vibrations. Therefore, the system is very suited of the OPF technique (Liu and Ohtsubo 1994a,b). We employ the OPF control system discussed in Fig. 9.3. Figure 11.19 shows the schematic diagram for

the OPF control in the active interferometer. From the detected output power from PD1, an appropriate sampling control signal is generated in the OPF control circuit with a synchronous signal (Sync Signal) and the control signal with a small amplitude is overlapped into photodetector PD2 for the fringe detection as a small perturbation. After successful control, the chaotic output of a laser oscillation is fixed to a periodic state.

Figure 11.20 is the experimental result of the OPF control. The delay time of the circuit is $\tau_e = 2.0\,\text{ms}$. Under the experimental condition, the laser exhibits chaotic oscillation as shown in Fig. 11.20a. The typical frequency of the chaotic signal is 0.24 kHz and it is almost equal to the sum of the times τ_i and τ_e. For the frequency of the synchronous signal in the control circuit of 2.64 kHz, the system is controlled to a periodic state. In Fig. 11.20b, the controlled waveform is the 11th harmonics of the fundamental period-1 orbit. On the other hand, the laser is controlled to the 7th harmonics of the fundamental period-1 orbit for the synchronous frequency of 5.04 kHz in Fig. 11.20c. The corresponding sampling frequency used as a control signal $g(t)$ is 21 multiples of the fundamental frequency. In delay differential systems, we can design and generate arbitrary multi-valued waveforms (isomer signals) of higher periodic orders for the fundamental periodic oscillation by adding extra control circuits to the systems (Liu and Ohtsubo 1991; Liu et al. 1994). In this example, the control signal is a very small perturbation to the chaotic oscillation and its amplitude is less than 3 % of the bias injection current. Therefore, the OPF control applied here is approximately considered as a category of chaos control in the meaning of the OGY algorithm. In the OGY method, the control signal is eliminated after the success of the control, but the control signal is continuously lasting with the same level. In the OPF method, the system must be always pushed by the control signal to fix a certain attractor of unstable periodic orbit.

References

Aoshima T, Ohtsubo J (1992) Two-dimensional vector LDV using laser diode frequency change and self-mixing effect. Opt Commun 92:219–224

Bosch T, Servagent N, Donati S (2001) Optical feedback interferometry for sensing application. Opt Eng 40:20–27

Donati S, Giuliani G, Merlo S (1995) Laser diode feedback interferometer for measurement of displacements without ambiguity. IEEE J Quantum Electron 31:113–119

Donati S, Falzoni L, Merlo S (1996) A PC-interfaced, compact laser-diode feedback interferometer for displacement measurements. IEEE Trans Instrum Meas 45:942–947

Durst F, Melling A, Whitelaw JH (1976) Principles and practice of laser Doppler anemometry. Academic Press, New York

Giuliani G, Norgia M (2000) Laser diode linewidth measurement by means of self-mixing interferometry. IEEE Photon Technol Lett 12:1028–1030

Giuliani G, Donati S, Passerini M, Bosch T (2001) Angle measurement by injection detection in a laser diode. Opt Eng 40:95–99

Giuliani G, Norgia M, Donati S, Bosch T (2002) Laser diode self-mixing technique for sensing applications. J Opt A Pure Appl Opt 4:S283–S294

Giuliani G, Bozzi-Pietra S, Donati S (2003) Self-mixing laser diode vibrometer. Meas Sci Technol 14:24–32
Gradshteyn IS, Ryzhik IM (1980) Table of integral, series, and products. Academic Press, New York
Groot PJ, Gaillatin GM (1989) Backscatter-modulation velocimetry with an external-cavity laser diode. Opt Lett 14:165–167
Lin FY, Liu JM (2004a) Chaotic radar using nonlinear laser dynamics. IEEE J Quantum Electron 40:815–820
Lin FY, Liu JM (2004b) Chaotic lidar. IEEE J Select Topics Quantum Electron 10:991–997
Liu Y (1994) Study of chaos in a delay-differential system with a laser diode active interferometer. Ph.D. thesis. Shizuoka University
Liu Y, Ohtsubo J, Shoji Y (1994) Accessing of high mode oscillations in a delayed optical bistable system. Opt Commun 105:193–198
Liu Y, Ohtsubo J (1991) Observation of higher-harmonic bifurcations in a chaotic system using a laser diode active interferometer. Opt Commun 85:457–461
Liu Y, Ohtsubo J (1992a) Chaos in an active interferometer. J Opt Soc Am B 9:261–265
Liu Y, Ohtsubo J (1992b) Period three-cycle in a chaotic system using a laser diode active interferometer. Opt Commun 93:311–317
Liu Y, Ohtsubo J (1993) Regeneration spiking oscillation in semiconductor laser with a nonlinear delayed feedback. Phys Rev A 47:4392–4399
Liu Y, Ohtsubo J (1994a) Experimental control of chaos in a laser-diode interferometer with delayed feedback. Opt Lett 19:448–450
Liu Y, Ohtsubo J (1994b) Controlling chaos of a delayed optical bistable system. Opt Rev 1:91–93
Merlo S, Donati S (1997) Reconstruction of displacement waveforms with a single-channel laser-diode feedback interferometer. IEEE J Quantum Electron 33:527–531
Mourat G, Servagent N, Bosch T (2000) Distance measurements using the self-mixing effect in a 3-electrode DBR laser diode. Opt Eng 39:738–743
Ohtsubo J, Liu Y (1990) Optical bistability and multistability in active interferometer. Opt Lett 15:731–733
Ohtsubo J, Kumagai H, Shogenji R (2009) Numerical study of Doppler dynamics in self-mixing semiconductor lasers. IEEE Photon Technol Lett 21:742–744
Okoshi T, Kikuchi K, Nakayama A (1980) Novel method for high resolution measurement of laser output spectrum. Electron Lett 16:630–631
Özdemir SK, Shinohara S, Takamiya S, Yoshida H (2000) Noninvasive blood flow measurement using speckle signals from a self-mixing laser diode: in vitro and in vivo experiments. Opt Eng 39:2574–2580
Scalise L (2002) Self-mixing feedback laser Doppler vibrometry. SPIE Proc 4827:374–384
Servagent N, Gouaux F, Bosch T (1998) Measurements of displacement using the self-mixing interference in a laser diode. J Opt 29:168–173
Shinohara S, Naito H, Yoshida H, Ikeda H, Sumi M (1989) Compact and versatile self-mixing type semiconductor laser doppler velocimeters with direction discrimination circuit. IEEE Trans Instrum Meas 38:674–577
Wang AB, Wang Y, He H (2008) Enhancing the bandwidth of the optical chaotic signal generated by a semiconductor laser with optical feedback. IEEE Photon Technol Lett 20:1633–1635
Yoshino T, Nara M, Mnatzakanian S, Lee BS, Strand TC (1987) Laser diode feedback interferometer for stabilization and displacement measurements. Appl Opt 26:892–897
Yu Y, Giuliani G, Donati S (2004) Measurement of the linewidth enhancement factor of semiconductor lasers based on the optical feedback self-mixing effect. IEEE Photon Technol Lett 16:990–992